OPTIMAL FUEL CONSUMPTION USING MULTILEVEL INVERTER BASED ANFIS RSC CONTROL STRATEGY ON WIND DRIVEN DFIG, DG AND SOLAR PV ARRAY

.Dr.RAMACHANDRA C G

[1-2,4-5]Department of Electrical and Electronics Engineering
[3]Department of Computer Science and Engineering
[1-6]JNTUA College of Engineering Pulivendula, Kadapa, India.
Corr.author mail: vempallerafi@gmail.com

Abstract:

In this article, a 7-level cascaded Multi-Level Inverter (MLI) and Adaptive neuro-fuzzy inference system (ANFIS) controller is the optimal fuel consumption of a Wind-driven power DFIG, DG, solar PV array, and Battery energy storage system by the grid. The purpose is to produce this microgrid system with a multilevel inverter, employing nearest-level control for lowering overall harmonic distortions and reducing bulk filters. It especially combines solar and winds renewable sources, which leads to an increase in output power and voltage. The ANFIS is control wind speed to develop torque with their respective references to improve dynamic performance with generated signals of PWM logic for the Rotor side converter (RSC). Modified perturb and Observe algorithms are used in this MPPT tracking for maximum power for wind and solar output with fewer or no oscillations. Using MATLAB software microgrid is designed and a simulation is done. A transient improvement throughout a large wind speed range can be accomplished by utilizing an ANFIS controller.

Keywords: adaptive neuro-fuzzy inference system (ANFIS), rotor side converter (RSC), multi-level inverter (MLI), optimal fuel, maximum power point tracking (MPPT)

1. Introduction:

The diesel generator (DG) sets implementation [1]is very popular use in islands, urban housing systems, and industries to back up power protection. The conversion efficiency is more than alternative energy sources to limit greenhouse gas emissions. DG's are used widely even if running is high, more noise and air pollution with the above benefits [2]. The operation cost of the plant is based on the power output using fuel, to reduce this cost renewable energy sources wind and solar using. The RE sources are free from pollution to nature, and wind and solar are used because with improving developing technologies, cost is also reduced [3].Wind turbines that are Double-fed induction generators (DFIG)are used to have volatile speed capability for wind energy to produce with low power loss [4].In the grid system, the author's majority's DFIG-based wind energy conversion system focuses on stand-alone [5], with operating battery energy storage (BES) back-to-back buck/boost connection connected directly to DC link. Author [6], discussed the functioning of wind turbine DFIG active power theory in balanced and unbalanced grid circumstances controlled by RSC. The voltage constantly adjusts with a Phased locked loop (PLL) [7], facilities of strength in grid connection. The synchronization control is to connect smooth operation in the grid [8], it is modified in IEEE39 bus system and has a requirement for a simulation platform. In another resource solar PV arrays have increasing power generation daily in multi nationals. The SECS or solar energy conversion system is single and double stages requires. Single-stage SECS [9] is connected to the grid for controlling fundamental current. In this grid double stage SECS [10] are used for a 7-level cascaded multilevel inverter, a basic current withdrawal approach situated on a generalized integrator of second order with a frequency-locked loop that has been designed.The7-level cascaded MLI reduces harmonics and its waveform in pure sinusoidal [11].

The WECS and SECS are both connected to the grid because of their economical and increasing power supply loyalty [12]. In this topology, A 7-level cascaded MLI with DC link, a bidirectional buck/boost converter, and a BES connects the DFIG and Solar PV arrays. In BES the capacity of battery improving with microgrid based on solar, wind, and DG in literature [13]. The BES has a major role to perform when load and generation are discrepancies. Moreover, the BES has an MPPT controller to control the power overflow charging and discharging to the load from solar and wind, these literatures are related to [14]. The purpose of the

diesel-wind-solar microgrid is to regulate and minimize DG fuel in order to achieve the best fuel efficiency across all output powers [15].The MLI, RSC controller has ANFIS controller [16] to control the wind speed to generate the power by DFIG. In Load Side Converter (LSC) to reduce the harmonics at PCC affected by the unbalanced loads in a grid. In order for this microgrid, DG fuel use should be optimized by taking maximum power drawn in solar and DFIG. In IEEE 519 standards, the stator currents of the DFIG and the DG currents in a point of common coupling (PCC) are kept balanced and sinusoidal. The design of DFIG, DG, and Solar PV array of microgrid-based BES are virtual, simulated in MATLAB simpower systems toolbox.

2. System Configuration:

The micro grid's illustrative structure as portrayed in Fig.1, utilizes a maximum capacity of 7.5 kW for a specific medium. The DFIG and DG are connected inline to a microgrid with fault protection of CB1 & CB2 correspondingly. DFIG is controlled by RSC and powered by a 7.5 kVA 4-pole synchronous generator, a 4-stroke combustion engine, and an automated voltage regulator (AVR). The solar PV array is pertaining to the voltage source controller(VSC) via the DC link capacitor, with the BES connected to the prevalent bus of a back-to-back coherent Buck/Boost DC-DC converter. The material reported in [12], [15], and [16] is used to develop wind turbines, solar generators, DG, BES, and other components. In addition, the microgrid model definition is included in Fig.1.

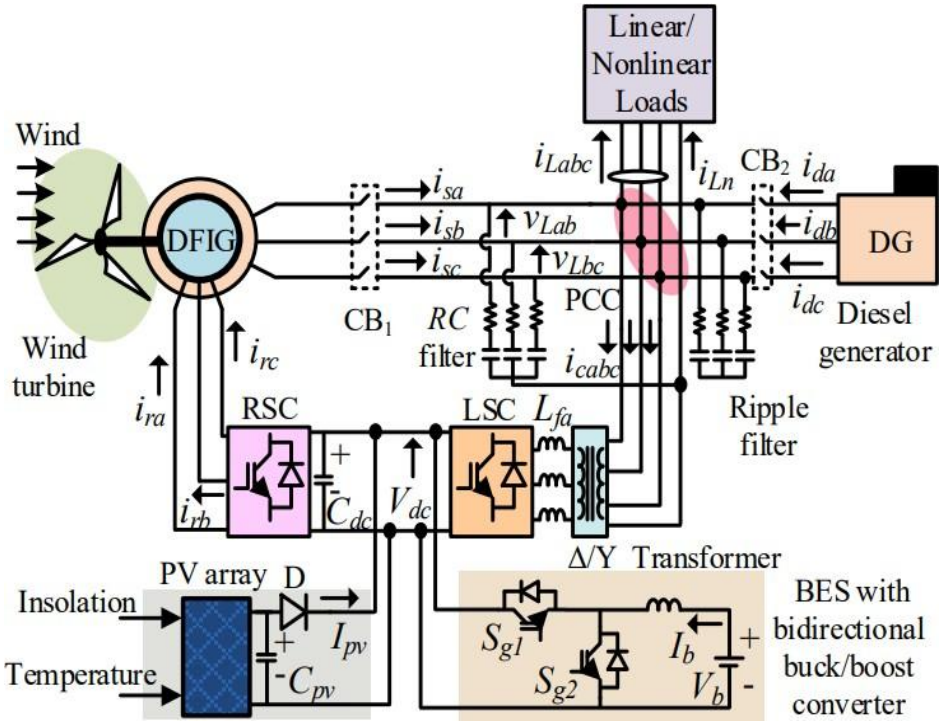

Fig.1DFIG microgrid

2.1 VSC and PI controller using Microgrid:

The 3-phase VSC controls RSC output current and DC-link Voltage control by using a PI controller and load side controller (LSC) to control DG &b DFIG stator currents to achieve sinusoidal and balanced. The selected Control is the PI controller, which is to accomplish system stability and DC voltage regulation, to control RSC speed error. PI controller has turned the disturbances that occurred when the sudden changes in load linear and non-linear loads, these disturbances are source increases or decreases in voltage, and similarly, load disturbances change in steady-state power demand minimizing the system disruptions that occurred.

3. CONTROL ALGORITHMS OF MICROGRID

Microgrid characterization control techniques are included below: RSC control, LSC control, MPPT algorithm for solar PV arrays, and control of bidirectional buck/boost DC-DC converters.

3.1 Control Algorithm for RSC:

In Fig 2, RSC control approach is illustrated. RSC is worn to afford reactive power enforced by the DFIG and to standardize the MPPT speed generated by wind turbine generators. The RSC must regularly meet DFIG reactive power requirements.

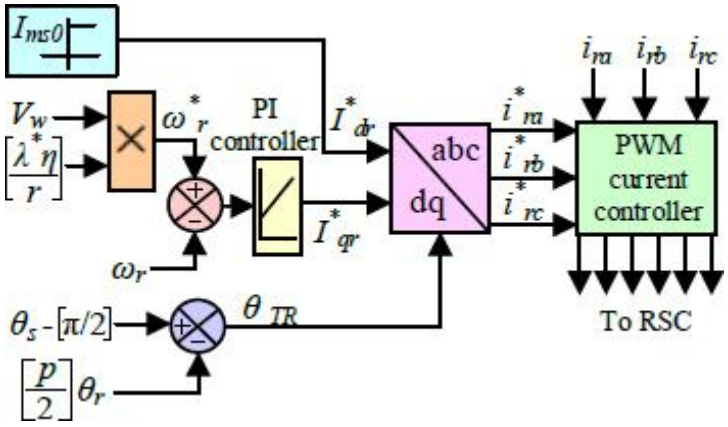

Fig.2: RSC Control Algorithm

The switching pulses are produced by RSC-adopted field-oriented vector control (FOVC), it has depicted in Fig. 2. In FOVC, the reactive and active components are represented by direct& quadrature axis (dq) components with inputs of rotor currents (I^*_{dr} , I^*_{qr}). I^*_{dr} Correlate DFIG's no-load magnetizing current (I_{ms0}) calculated as [21]

$$I_{ms0} = \frac{\sqrt{2}V_L}{\sqrt{3}X_m} \quad (1)$$

WhereX_m, V_L is the machine's magnetizing reactance and at the machine's terminals, line voltage respectively.

The $I^*_{qr}$is calculated away fleeting speed error concluded PI controller has portrayed in Fig. 2, calculated as

$$I^*_{qr(k)} = I^*_{qr(k-1)} + K_{p\omega}(\omega_{err(k)} - \omega_{err(k-1)}) + K_{i\omega}\omega_{err(k)} \quad (2)$$

$K_{p\omega}$ and $K_{i\omega}$are the PI speed controller constants and $\omega_{err(k)}$&$\omega_{err(k-1)}$are represented as speed errors at $K_{th}$and $(K-1)_{th}$levels subsequently.

The $\omega_{err(k)}$is calculated by

$$\omega_{err(k)} = \omega^*_{r(k)} - \omega_{r(k)} \quad (3)$$

$\omega^*_{r(k)}$, $\omega_{r(k)}$arerepresent DFIGK_{th}reference and sensed rotor speed.

MPPT control Tip speed ratio (TSR) [19] as to find reference rotor speed (ω^*).

$$\omega^*_r = \eta\boldsymbol{\lambda}^*\mathbf{V}\ /\mathbf{r} \quad (4)$$

V_w, $\boldsymbol{\lambda}^*$, η and r Stands for wind speed, ideal tip speed ratio, gear ratio, and wind turbine radius, subsequently. The rotor transformation angle (θ_{TR})is determined as,

$$\theta_{TR} = (\theta_s - \frac{\pi}{2}) - (\frac{P}{2})\theta_r \quad (5)$$

In which$\theta_s$is acquired phase locked loop and $\theta_r$be tailed in distinction to detected rotor speed just as,

$$\theta_r = \int_0^t (\omega_r)dt \quad (6)$$

Finally, as shown in Fig.2, reference rotor currents (i^*_{ra}, i^*_{rb} and i^*_{rc}) are sourced taken awayI^*_{qr} and I^*_{dr} utilizing a transformation angleθ_{TR}. These benchmark currents, facing conjunction along detected rotor currents (i_{ra}, i_{rb} and i_{rc}), utilized to generate RSC gating signals using pulse width modulation (PWM).

3.2 Control Algorithm for LSC:

LSC's control algorithm method is shown in Fig.3.With LSC controller towards maintain sinusoidal and balanced DG and DFIG stator currents. To achieve optimal fuel consumption DG power range with in PD_{min}toPD_{max}, it refers to DG power outputs minimum and maximum in pu.
In order to produce the reference currents in the act of illustrated in Fig.3 by the modified indirect vector control due to voltage-oriented reference frame. The total of DG and DFIG stator currents are added together and DFIG power is fragmented at its highest level under control, while DG power is managed within bounds to ensure optimal fuel consumption. The d-axis element as regards LSC is calculated by

$$I^* = I^* + I^* \quad (7)$$

Where I^* ,I^* are represent as d-component current as concerns DG and DFIG correspondingly to Operating DG optimum fuel-efficient zone when load changes, a block of saturation are placed before the I^* component is completed.

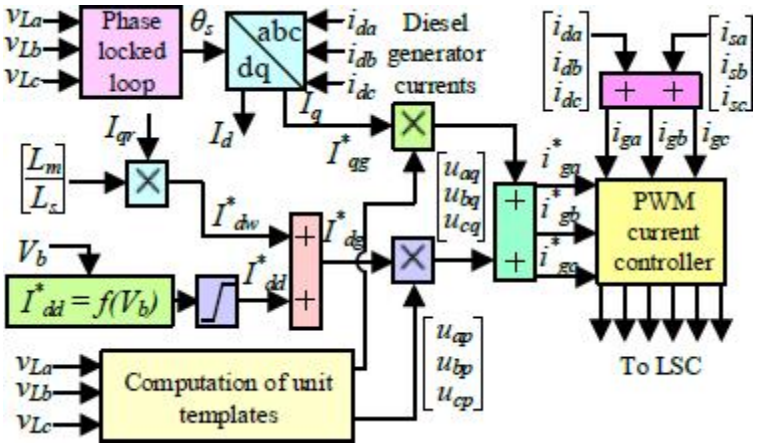

Fig.3: LSC control algorithm

In the above equation I^* andI^* are computed as

$$I^*_{dd} = \left(\frac{(\sqrt{2}/3)*P^*_D*VA_{DG}}{V_L}\right) \quad (8)$$

$$I^* = \left(\frac{L_m}{}\right) I \quad (9)$$

In (8), where VA_{DG} and V_L are the base values of DG VA rating and line voltage found in PCC respectively and P^*_D is the DG power in pu, it is a broad term that is used to compute based on the status of the BES. and determined as,

$$P^*_D = P^*_{Dmin} + k_1\beta \quad (10)$$

From (10) the rate of varies among 0 and 1. Voltage at the BES's complete charging is minimal amount and BES is in minimum voltage then is maximum value. has the form

$$\beta = \frac{V_{bmax} = V_b}{2} \tag{11}$$

In (10) and (11), k_1 and k_2 denote constant parameters. P_D^* is chosen to achieve its highest limit of optimal fuel usage as a contribution to unity, and k_2 is chosen to achieve unity at V_{bmin}. The values of PD_{min}, PD_{max}, V_{bmax}, V_{bmin}, k_1 and k_2 used in this study are listed in the appendices.

The DG currents (, and) are translated directly towards$I_d$and I_q values are taken from PLL using angle of transformation (θ_s) as portrayed in Fig. 3. LSC current's q-axis component (I_{qg}^*) is quantitatively equivalent to DG'sI_q. To produce current references,$I_{dg}^*$and I_{qg}^*values held by in-phase and quadrature unit templates are multiplied subsequently, after which they are assembled to produce reference currents (i_{ga}^*, i_{gb}^* and i_{gc}^*). The phase voltages (, and) were derived from to create the unit templates, which are produced as,

$$= \frac{-}{v}, \quad = \frac{-}{v}, \quad = \frac{-}{v} \tag{12}$$

Peak phase voltage ( ) at PCC is measured by,

$$= \{ \frac{2(\ ^2 + \ _b^2 + \ _c^2)}{3} \}^{1/2} \tag{13}$$

The group of arrangements in quadrature components on the basics of in-phase elements as,

$$u \quad = -\frac{\omega_{bp}}{\sqrt{3}} + \frac{\omega_{cp}}{\sqrt{3}}, u \quad = \frac{\omega_{ap}}{2} + \frac{\omega_{bp} - \omega_{cp}}{2\sqrt{3}}, ucq = -\frac{\omega_{ap}}{2} + \frac{\omega_{bp} - \omega_{cp}}{2\sqrt{3}} \tag{14}$$

Finally, as illustrated in Fig. 3, the produced reference currents and detected currents (, and),LSC pulses are created by being delivered to the PWM controller.

3.3 Solar PV Array MPPT Algorithm and Bidirectional Buck/Boost DC-DC Converter Control:

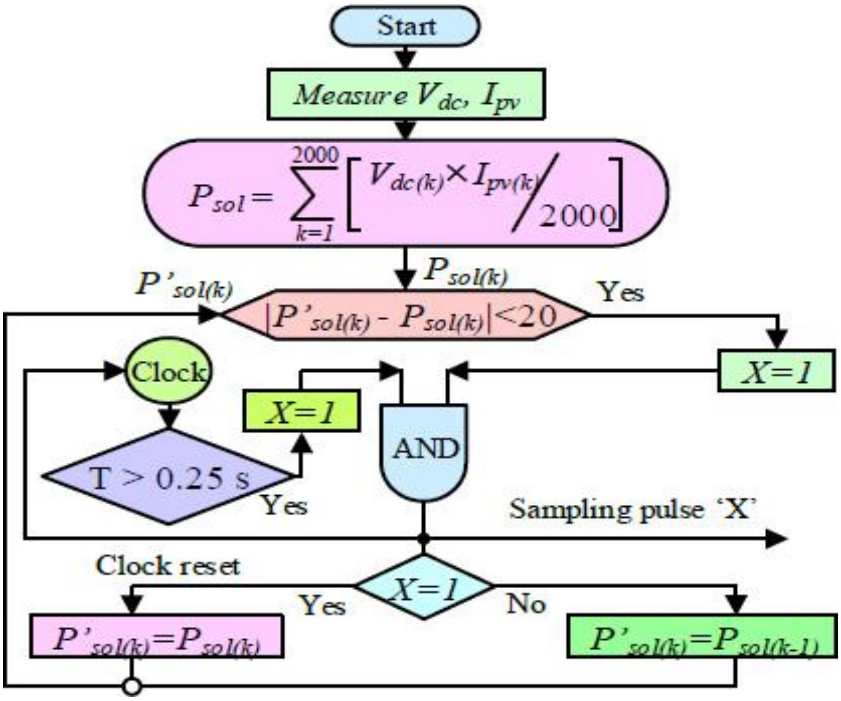

Fig.4: Sampling Pulse generation

BES is a controlled power flow of a DC-DC converter that is bidirectional Buck/Boost regulates the DC link voltage, by execution this solar MPPT still achieved. Here a modified perturb and observe (P&O) algorithm is utilized to found appropriate sampling pulse generation (X) together with finally calculate reference DC link voltage (V_{dc}),according to flowcharts Fig.4 & Fig.5. Individual steps required to generate sampling pulse 'X' is depicted in Fig.4. X varies digit bits from 0 to 1.

In Fig. 4, the first step is to measure at k^{th} instant, the voltage of DC link or solar PV voltage (V_{dc}) and solar PV current (I_{pv}). The second step is calculation of mean solar power (P_{sol}) by taking first step instantaneous values of kth solar PV voltage and current, it serves the same purpose as filtering. With the average solar power (P_{sol}) and formerly indicated power (P'_{sol}) difference is less than 20W combined previous sampling of minimal time delay 0.25s, Control detects the onset of steady state. When output has steady state, the sampling pulse 'X' turns into 1. The gradual adjustment in the reference solar PV MPPT voltage (V^*_{dc}) was started individually sampling pulse, it updates only conceding that sampling pulse becomes'1'.

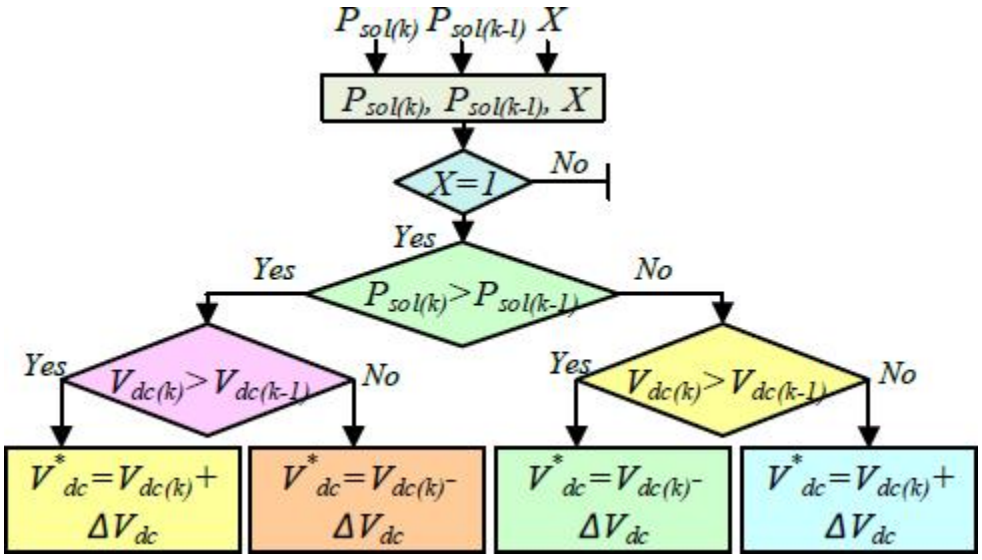

Fig.5: MPPT algorithm of solar PV array

In Fig.5 clear conspicuous this shows the altered modified P&O MPPT algorithm. When X changes to '1', the MPPT algorithm checks to see whether$P_{sol(k)}>P_{sol(k-1)}$. If yes, it will be check again $V_{dc(k)}>V_{dc(k-1)}$. The new reference solar PV voltage is $V^*_{dc} = V_{dc(k)} + \Delta V_{dc}$ if the answer to both questions is yes. where ΔV_{dc} represents the little increase in solar PV voltage.

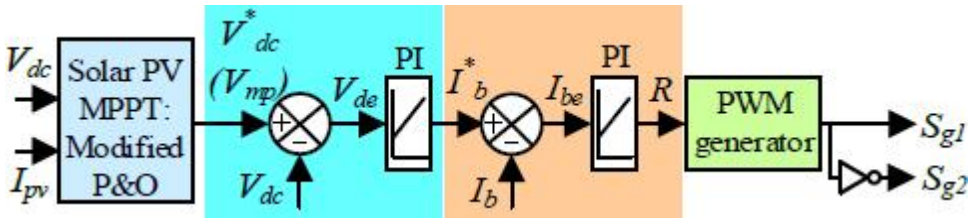

Fig.6: control of bidirectional buck/boost converter

In Fig.6 illustrated is controlled on the way bidirectional buck/boost DC-DC converter. To find the DC link voltage in exterior bidirectional buck/boost converter's proportional-integral (PI) controller. Reference battery current (I^*_b) of constitutional PI controller is the output of outer PI controller. Essential PI controller for tracking

reference battery current and the output is the bidirectional buck/boost converter's duty ratio (R).Current against a reference battery as

$$I^{*}_{b(k)} = I^{*}_{b(k-1)} + K_{pb}(V_{de(k)} - V_{de(k-1)}) + K_{ib}V_{de(k)} \quad (15)$$

Where, error attribute to the solar PV voltage towards k^{th} instant is$V_{de(k)} = V^{*}_{dc(k)} - V_{dc(k)}$. Here $V^{*}_{dc(k)}$ and $V_{dc(k)}$serve the mentioned DC link voltage and detected DC link voltage appearing in k^{th} moment, respectively. K_{pb} and K_{ib}serve as a basis for the proportional and integralconstitutional PI controller. Along with, the duty ratio (R) away from the bidirectional DC-DC converter, is reckoned as, integral restrictions of the exterior PI controller.

$$R_{(k)} = R_{(k-1)} + K_{pr}(I_{be(k)} - I_{be(k-1)}) + K_{ir}I_{be(k)} \quad (16)$$

Where $I_{be(k)} = I^{*}_{b(k)} - I_{b(k)}$ is the glitch of the battery current at the k^{th} prompt. $I^{*}_{b(k)}$ and $I_{b(k)}$perform the mentioned and detected battery currents at the k^{th} moment, respectively.The gathered duty ratio (R) be alive sent into the PWM generator, which generates pulses for the bidirectional converter, either buck or boost switches.

4. Proposed Method:

4.1 Multi-level inverter with ANFIS controller in micro grid:

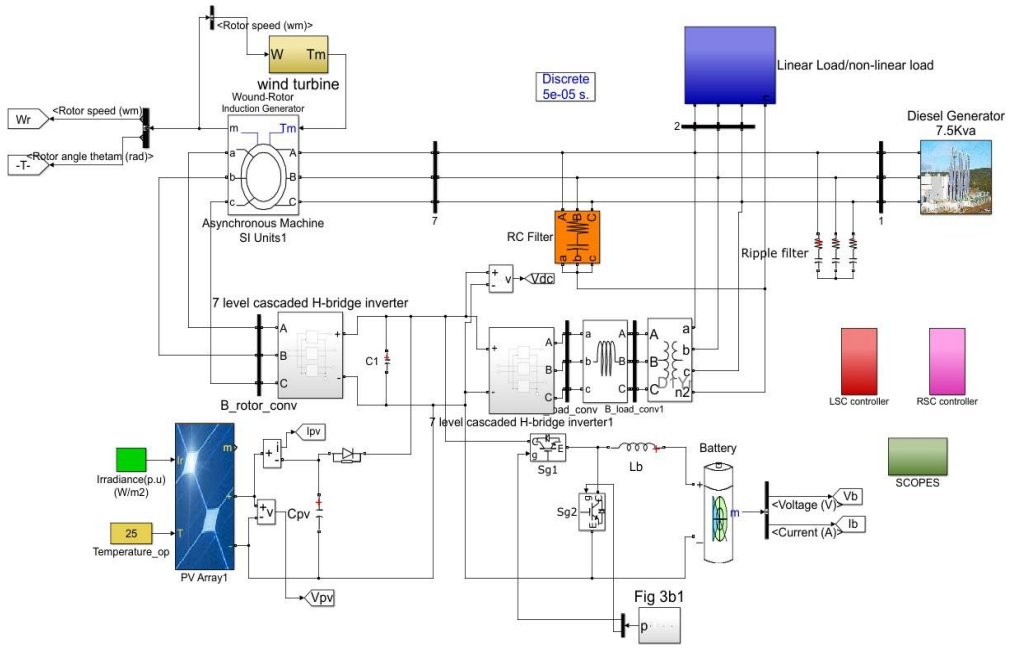

Fig.7: 7-level cascaded MLI microgrid

In this technique, we are using 7-level cascaded multi-level inverter in place of two-level voltage source converter shown in fig.7, why in fact to use MLI because VSC has poor efficiency in medium and high voltage application, mainly power loss across switches. Hence to reduce this problem MLI is used. As number of levels in MLI increases, THD will be reduced and getting pure sinusoidal wave form but the power modules increased. This leads to complexity between switches and power supply. Hence, this work proposed a 7-level MLI with reduced switches. In cascaded 7-level MLI includes 3-H bridges, 12 IGBT switches are to produce output is shown in fig.8.

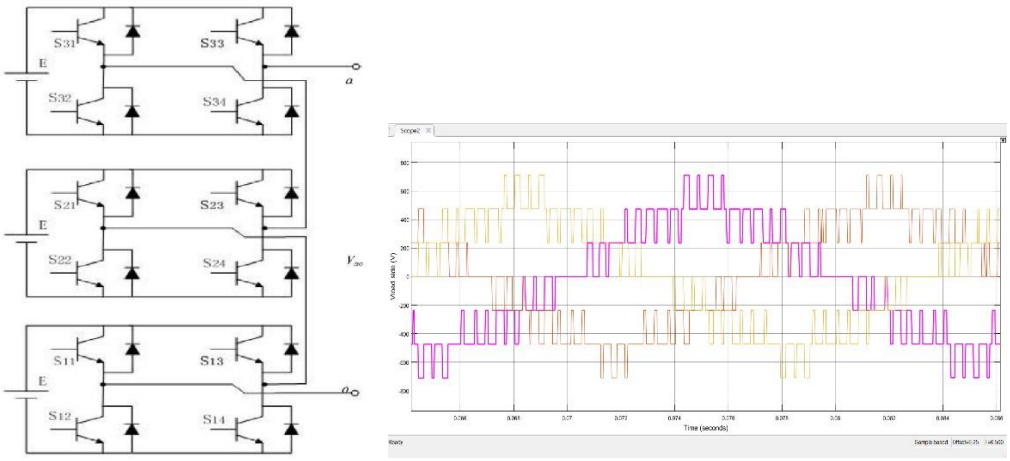

Fig.7: 7-level cascaded multilevel inverter

4.2 ANFIS Controller:

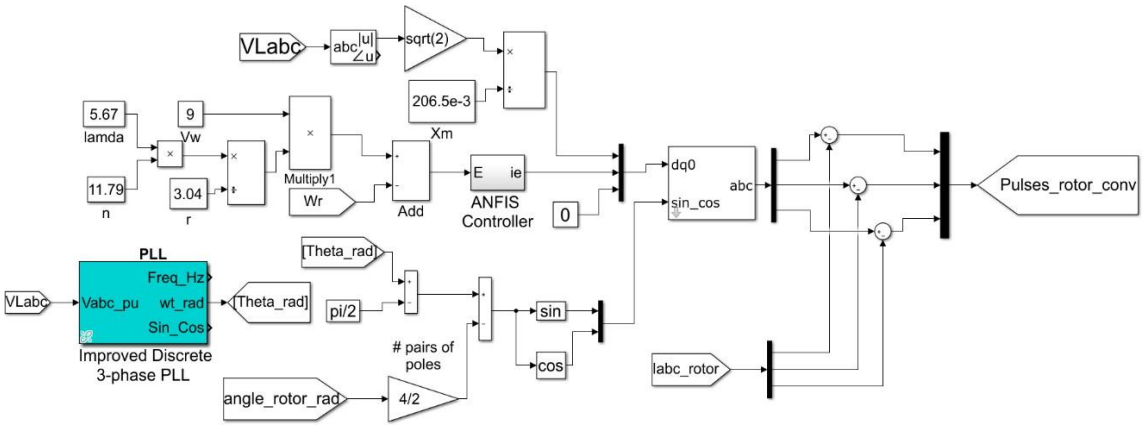

Fig.9: ANFIS controller in RSC

PI controllers sudden change in RSC cannot adjust KP & KV values, which are poor performance of rapid changes in DFIG-WECS. More difficult to changing linear or non-linear loads control in emergency. The PI controller's performance suffers when the machine parameters are changed while operating under varied conditions and the pattern values must be updated with each change. Due to this adaptive neuro-fuzzy inference system (ANFIS) is a fuzzy inference system whose membership functions may be recreated using a genuine input-output data set as shown in fig.10. The ANFIS controller to control the wind speed in RSC appears in Fig.9.

According to the Takagi-Sugeno fluffy inference framework, an adaptable neuro-fuzzy inference system (ANFIS), also known as a flexible organization-based fluffy induction framework, is a manufactured brain network. ANFIS is divided into six levels, as indicated in fig. First layer is taken input values from system. The second layer is a fuzzification, which collects data values from the system and determines the associated participation capabilities. The third layer is a rules layer, which may standardise the figured terminating quality by dividing each value by the overall terminating strength. The fourth layer receives the results of normalised boundary output values of membership functions, and the final layer returns the final output values as defuzzification.

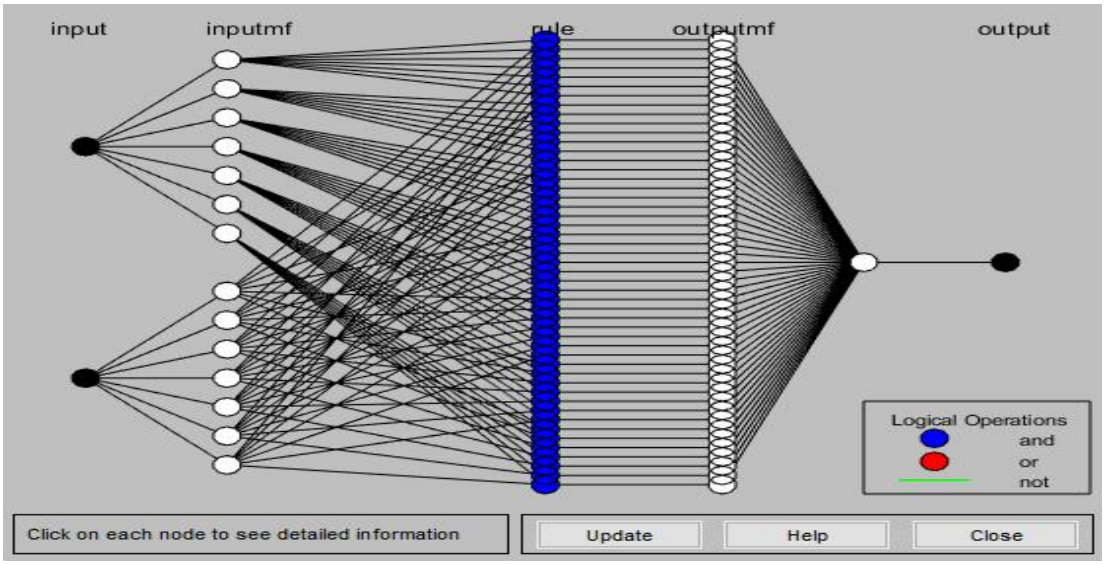

Fig.10: Structure of ANFIS

5. SIMULATION RESULTS:

7-level cascaded MLI microgrid is simulated in MATLAB. In a system performance of Various signals are$V_r$be the phase voltage's rms value, $f_L$be the system frequency, $w_r$be the DFIG rotor speed,P_D be the DG power, P_w be the wind power from stator, P_{PV} be the solar PV power, P_L be the load power, PLSC be the LSC power, V_{dc} be the DC link voltage, $I_b$be the battery current, V_b be the battery voltage, V_w be the wind speed, G be the insolation, C_p be the rotor power co-efficient, i_{sa} be the a-phase stator current, i_{rabc} be the rotor currents, i_{da} be the a-phase DG current, V_{La} be the a-phase PCC voltage, i_{sabc} be the DG currents, (i_{La}, i_{Lb}, i_{Lc}) be the load currents, i_{Ln} be the neutral currents and i_{cabc} be the LSC currents. The parameters of the simulation are presented in Appendices.

5.1 Performance of Bidirectional Buck/Boost DC-DC converter at change in Load:

When the load in the PCC is adjusted, the conducting of a bidirectional Buck/boost DC-DC converter is displayed in Fig11. A 2.5 KW 3-phase balanced load was initially connected at PCC. The corresponding power distributed 2.5 kW load by the solar PV, DFIG and DG are 4.122 KW, 2.013 KW, 4.84 KW respectively, with excessive power storage to battery voltage of 125v BES through bidirectional buck/boost DC-DC converter is depicted in Fig.11. In this period, the generation power of any remaining sources is growing, and a steady load is handled via LSC through BES. The DC link voltage in fig 11 has reduced sag and swell, but the solar MPPT is unchanged, as seen by the waveform in Fig.11 and the system voltage and frequency remained steady, THD is reduced.

5.2 System performance at Variable wind speeds:

When the variable wind speeds are controlled, a 4 KW 3-phase load DG power of 5.76 is presented in Fig.12, insolation is kept at 700 W/m2, and the system is linked at PCC. At time t=3sec wind speed changes 7m/s to 7.5m/s and t=6.5sec wind speed decreases 7.5m/s to 6.5m/s is shown in Fig.12 (a). In Fig.12 (a), controller regulated the rotor speed of DFIG obeys as per wind power MPPT algorithm and DC link voltage. The ANFIS-based adaptation scheme's broad speed response provides good dynamic and steady-state performance. In Fig.12(b) shows the dynamic response of system over the changeover of DFIG speed changes

to super synchronous to sub synchronous speed zone. LSC power is changing due to effect of varying wind speed as shown in Fig.12 (b). The frequency of the rotor currents varies with the DFIG's operational speed.

5.3 System Performance at Variable Insolation:

Fig.13(a-b) shows the system's performance under various levels of solar insolation, a 4 KW 3-phase load is connected at PCC, wind is maintained 7m/s, DG power of 4.2 KW depending on the current status of BES. As demonstrated in Fig.13(b), solar PV insolation changes from 700 W/m^2 to 800 W/m^2 at t=3 sec and from 800 W/m^2 to 600 W/m^2 at t=5.5 sec. The bidirectional DC-DC converter modulates the DC link voltage to accomplish solar power MPPT, this characterizes in P_{sol} waveform in Fig.13(b)

5.4 System Performance at Unbalanced Nonlinear Load:

Fig.14 (a) depicts the system's dynamic performance when subjected to an uneven nonlinear load. At PCC, a 6.7 kW power supply with a balanced load is initially attached. It has a linear load of 0.5 kW and a nonlinear load, which is coupled to each phase. Phase-a of the load is disconnected at t = 2.6 s, and phase-b connection is lost at t = 2.8 sec, as shown in Fig. 14(a). The DFIG and DG voltages and currents are balanced and adhere to the IEEE 519 standard. The LSC aids in the adjustment of imbalance and harmonics in the linked load at the PCC. Fig. 14(b) illustrates the neutral current and LSC current as well. The unbalanced linear loads for varying power waveforms are shown in Fig.14 (b), from this generation sources are unaffected even in unbalanced loads. When the load power diminishes, the LSC controller sends surplus power to the BES, as demonstrated in the waveforms of , , and , Vr is held resolute value.

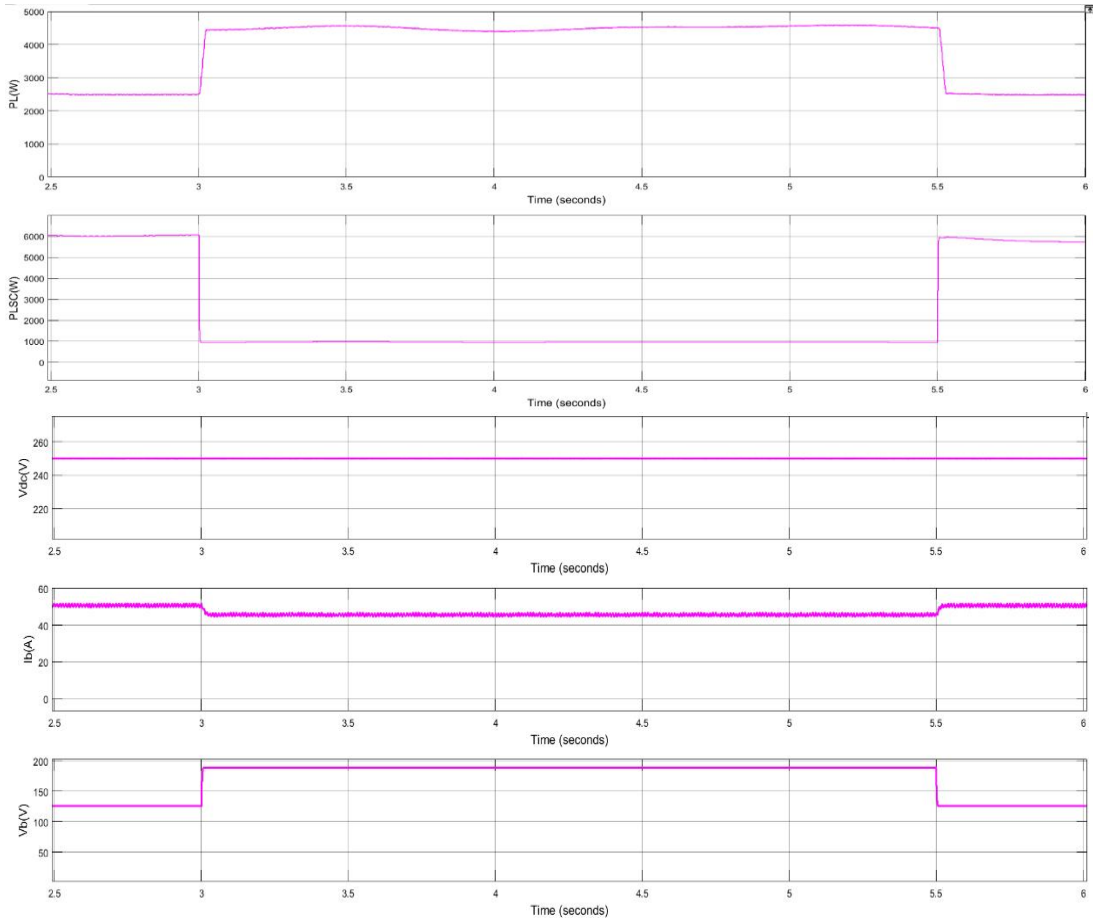

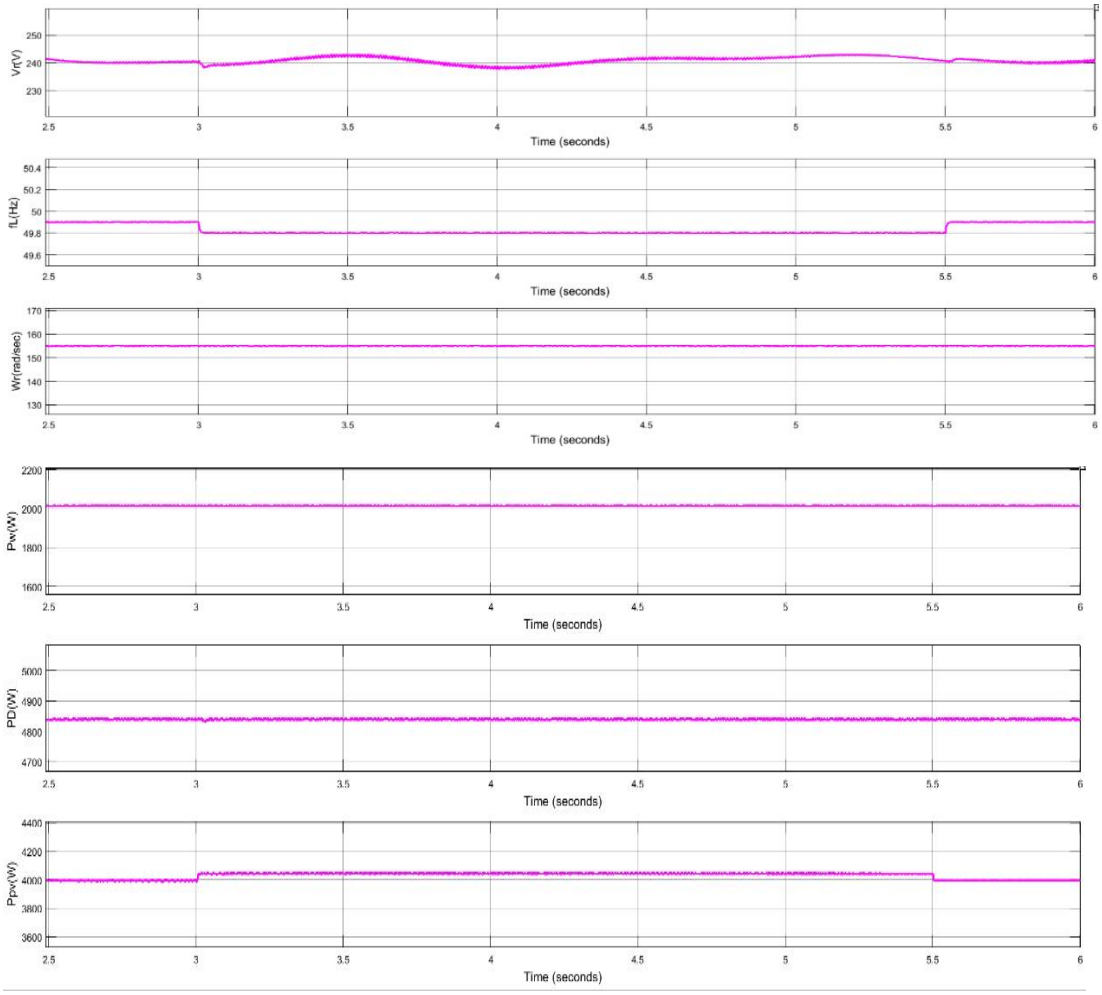

Fig.11. Performance of bidirectional buck/boost converter at change in balanced load

, , , I , , ,f , , , and

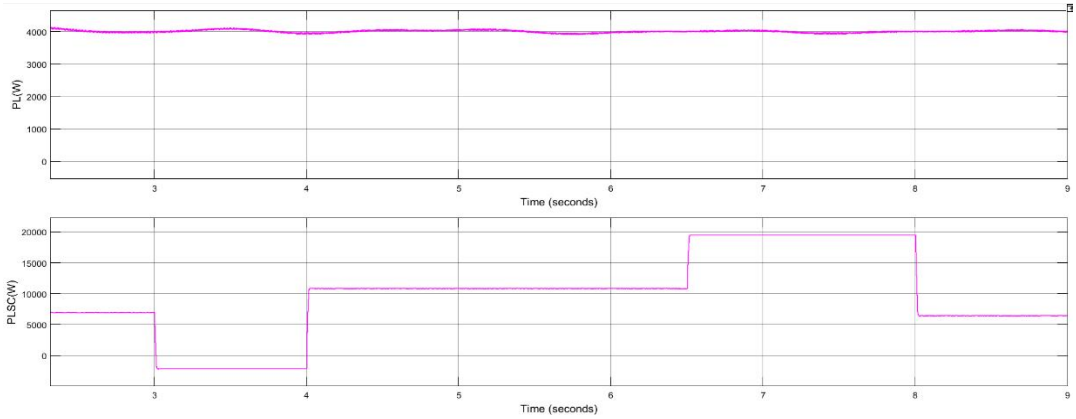

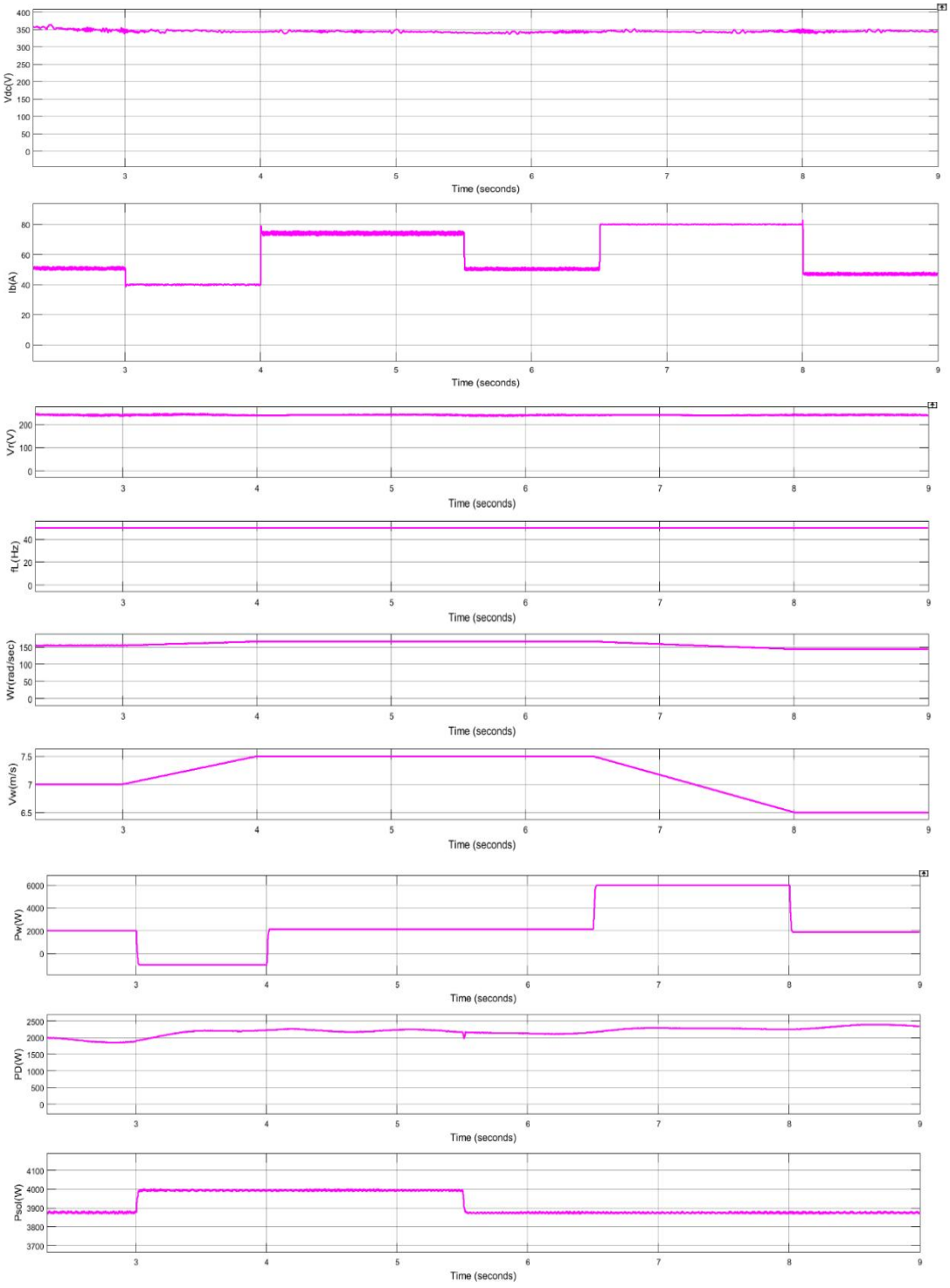
Vdc(V)
Time (seconds)
Ib(A)
Time (seconds)
Vr(V)
Time (seconds)
fL(Hz)
Time (seconds)
Wr(rad/sec)
Time (seconds)
Vw(m/s)
Time (seconds)
Pw(W)
Time (seconds)
PD(W)
Time (seconds)
Psol(W)
Time (seconds)

(a)

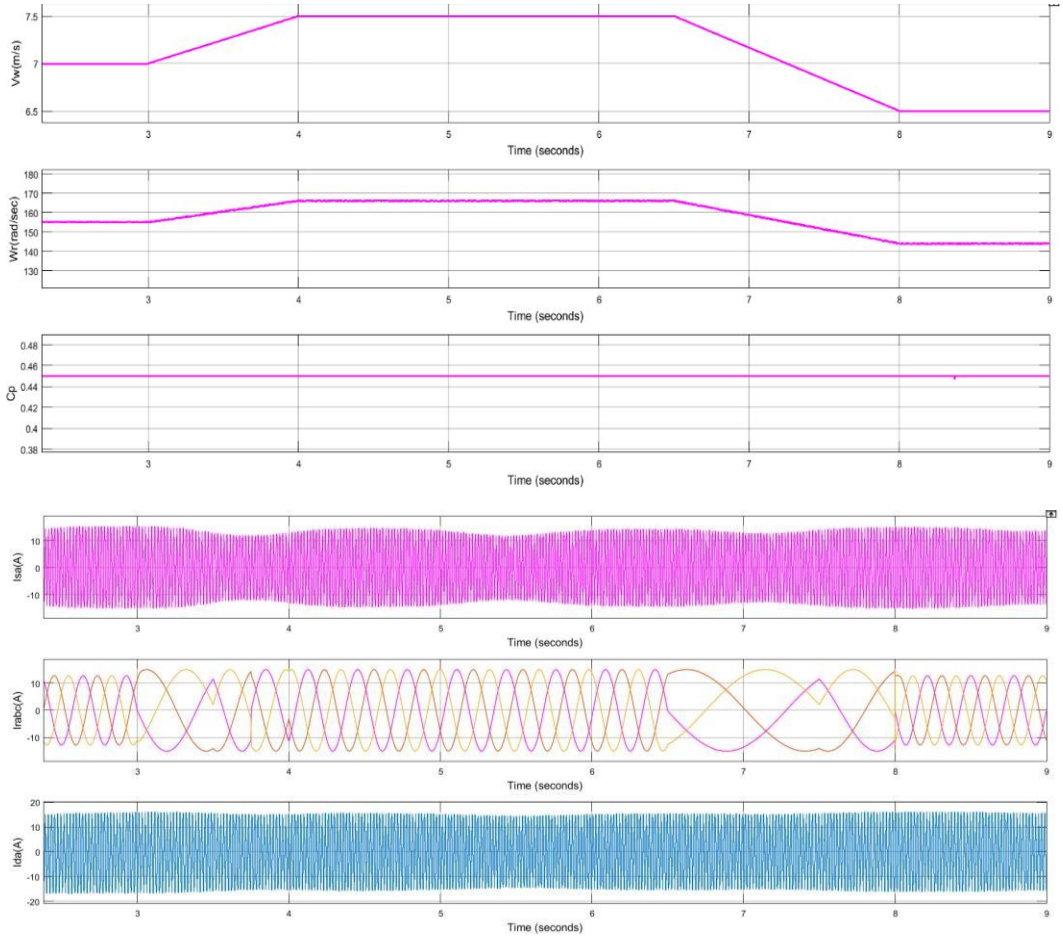

(b)

Fig.12. System performance at variable wind speed (a) , , , , ,f , , , , , and (b)

, , , , ,

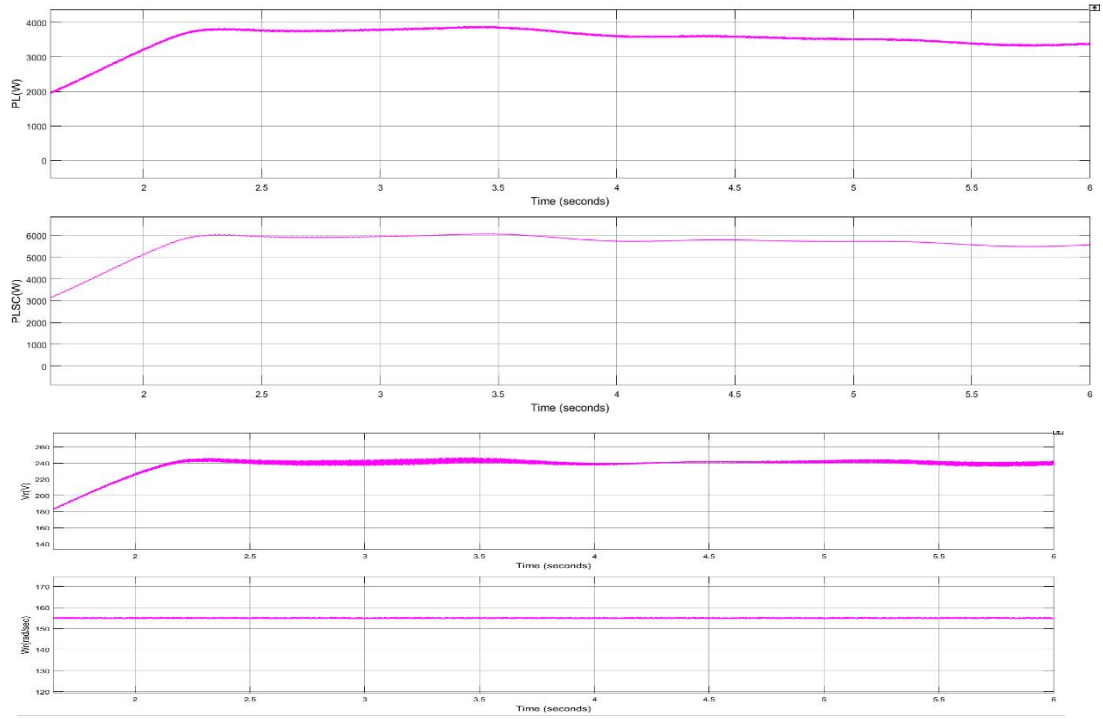

(a)

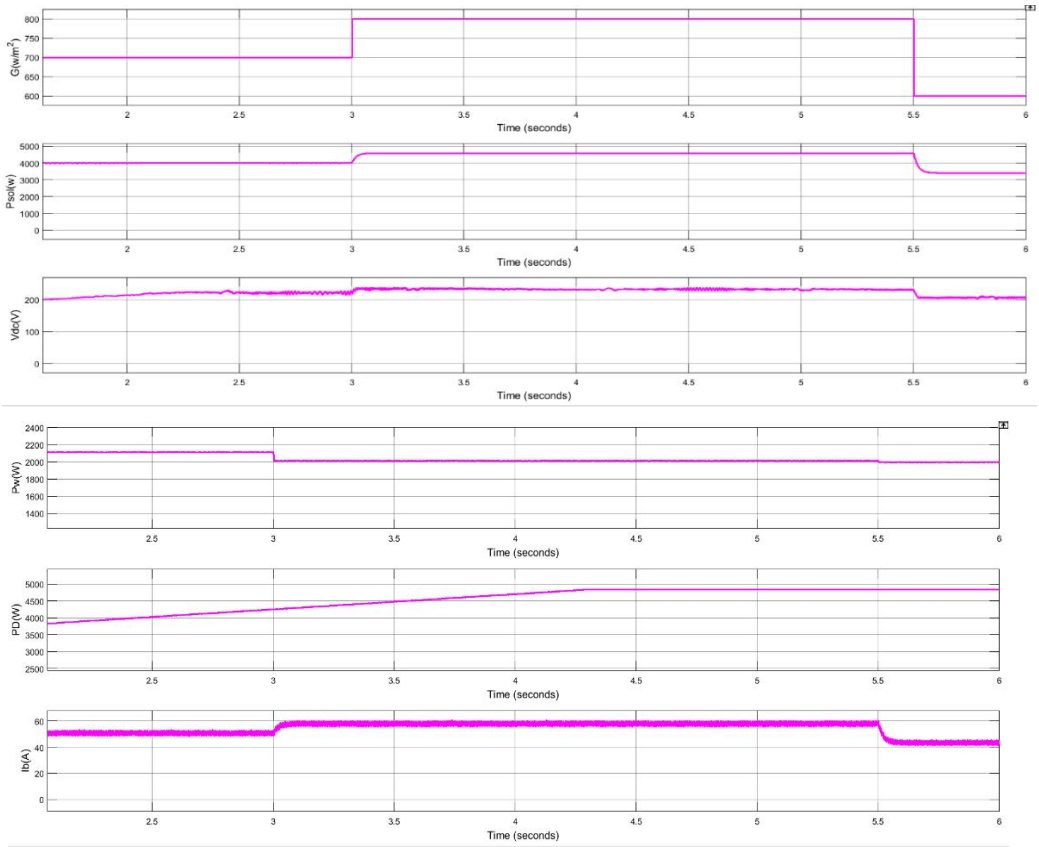

(b)

Fig.13. System performance at variable insolation (a) , , , and (b) G, , , , ,

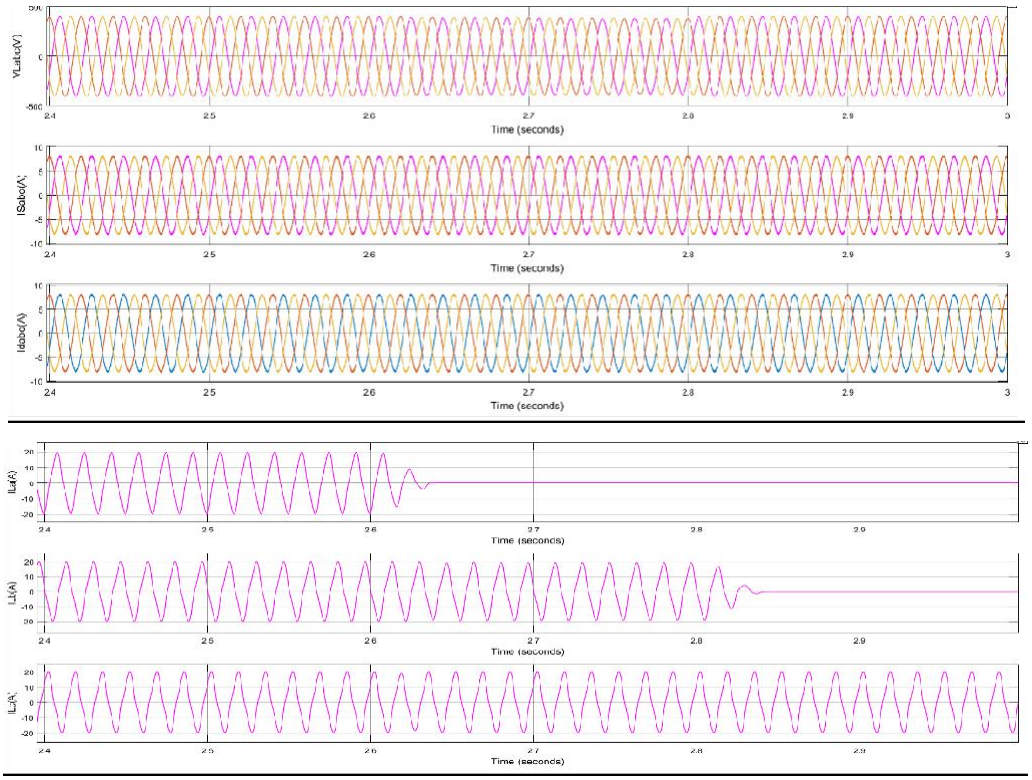

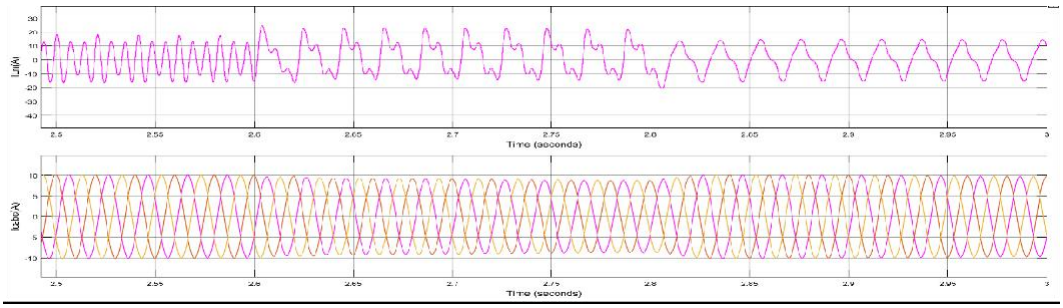

(a)

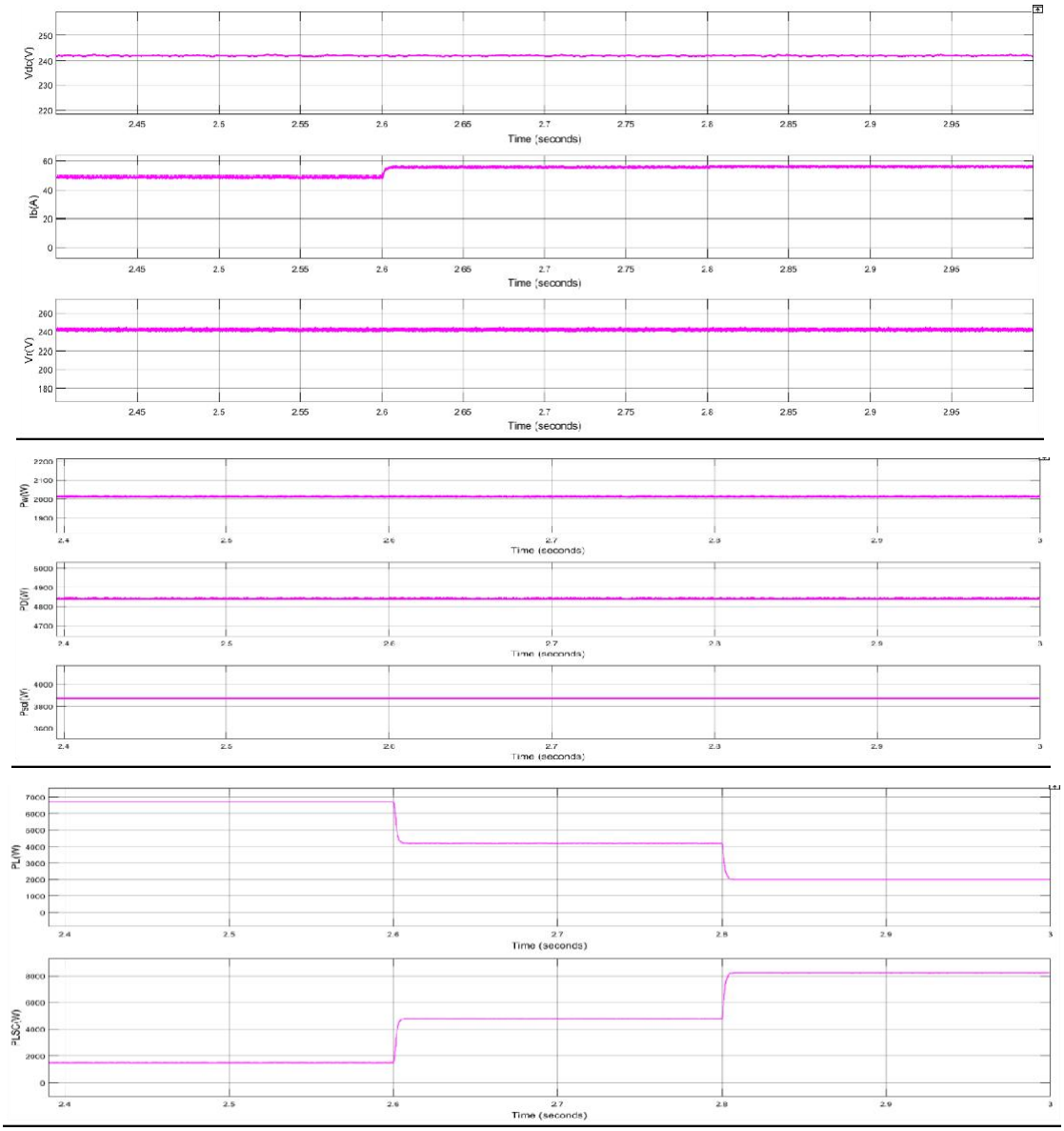

(b)

Fig.14. (a) System voltages and currents at unbalanced nonlinear load: , , , , , , , , and (b) system balanced at nonlinear unbalanced load: , , , , , , ,

6. Conclusion:

A 3-phase, 7-level multi-level inverter with an ANFIS controller is built into the RSC for micro grids. The design of MLI holds several advantages in characteristic topology for the reduction of power components in an affordable way. ANFIS was designed for precision and has been trained to provide quick and accurate results. It increases the transient response of DFIG based on various wind speeds. MLIs are mostly used in medium-voltage applications and micro grids powered by renewable energy sources. Simulated results show good performance to achieve optimal fuel consumption. It is discovered that the DFIG stator voltages, currents, and DG currents are sinusoidal and balanced in accordance with IEEE 519. In every case, the micro grid's regulation effectiveness with voltage and current THD is less than 4%. Using the intimate method, fluctuations in frequency can be successfully reduced, removing third harmonics.

References:

1. J. Knudsen, J. D. Bendtsen, P. Andersen, K. K. Madsen, and C. H. Sterregaard, "Supervisory control implementation on diesel-driven generator sets," IEEE Trans. Ind. Electron., vol. 65, no. 12, pp. 9698-9705, Dec. 2018.
2. J. Jo, H. An, and H. Cha, "Stability improvement of current control by voltage feedforward considering a large synchronous inductance of a diesel generator," IEEE Trans. Ind. Applicat., vol. 54, no. 5, pp. 5134- 5142, Sept.-Oct. 2018.
3. T. Adefarati, R. C. Bansal, and J. John Justo, "Techno-economic analysis of a PV–wind–battery–diesel standalone power system in a remote area," The Journal of Engineering, vol. 2017, no. 13, pp. 740-744, 2017.
4. C. Wu and H. Nian, "Stator harmonic currents suppression for DFIG based on feed-forward regulator under distorted grid voltage," IEEE Trans. Power Electron., vol. 33, no. 2, pp. 1211-1224, Feb. 2018.
5. N. K. Swami Naidu and B. Singh, "Experimental implementation of doubly fed induction generator-based standalone wind energy conversion system," IEEE Trans. Ind. Applicat., vol. 52, no. 4, pp. 3332-3339, July-Aug. 2016.
6. D. Sun, X. Wang, H. Nian, and Z. Q. Zhu, "A sliding-mode direct power control strategy for DFIG under both balanced and unbalanced grid conditions using extended active power," IEEE Trans. Power Electron., vol. 33, no. 2, pp. 1313-1322, Feb. 2018.
7. Ju Liu, Wei Yao, Jinyu Wen, Jiakun Fang, Lin Jiang, Haibo He, and Shijie Cheng, "Impact of power grid strength and PLL parameters on stability of grid-connected DFIG wind farm," IEEE Trans. Sustain. Energy, vol. 11, no. 1, pp. 545-557, Jan. 2020.
8. A. Thakallapelli, S. Kamalasadan, K. M. Muttaqi, and M. T. Hagh, "A synchronization control technique for soft connection of doubly fed induction generator based wind turbines to the power grids," IEEE Trans. Ind. Applicat., vol. 55, no. 5, pp. 5277-5288, Sept.-Oct. 2019.
9. P. Shah, I. Hussain, and B. Singh, "Single-stage SECS interfaced with grid using ISOGI-FLL-based control algorithm," IEEE Trans. Ind. Applicat., vol. 55, no. 1, pp. 701-711, Jan.-Feb. 2019.
10. A. K. Singh, I. Hussain, and B. Singh, "Double-stage three-phase gridintegrated solar PV system with fast zero attracting normalized least mean fourth based adaptive control," IEEE Trans. Ind. Electron., vol. 65 , no. 5, pp. 3921-3931, May 2018.
11. R. Arulmozhiyal , Dr. M.Murali , and K.R. Manjeri, "Design and Analysis of 7 Level Multilevel Inverter for Industrial Applications," Turkish Journal of Computer and Mathematics Education., Vol.12 No.9, pp.2777-2781, Jan 2021.
12. M. J. Morshed and A. Fekih, "A novel fault ride through scheme for hybrid wind/PV power generation systems," IEEE Trans. Sustainable Energy, Early Access.
13. Y. Zhang, J. Wang, A. Berizzi, and X. Cao, "Life cycle planning of battery energy storage system in off-grid wind–solar–diesel microgrid," IET Gener., Trans. & Distr., vol. 12, no. 20, pp. 4451-4461, Nov. 2018.
14. J. Hussain and M. K. Mishra, "Adaptive maximum power point tracking control algorithm for wind energy conversion systems," IEEE Trans. Energy Convers., vol. 31, no. 2, pp. 697-705, June 2016
15. S.Puchapalli, S.K.Tiwari, B.singh, and P.K.Goel, "A microgrid based on wind driven DFIG,DG and solar PV array for optimal fuel consumption," in IEEE Transactions on Industry Applications, (Volume: 56, Issue: 5, Sept.-Oct. 2020)
16. M.R. Mohanraj, R. Prakash, "Research and Control of STATCOM using ANN and ANFIS," International Journal of Recent Technology and Engineering (IJRTE) ISSN: 2277-3878, Volume-8, Issue-2S11, September 2019.